Robust Dynamical Decoupling for the Manipulation of a Spin Network Via a Single Spin

Xiaodong Yang,[1,2,3] Yunrui Ge,[1,2,3] Bo Zhang,[4,*] and Jun Li[1,2,3,†]

[1] *Shenzhen Institute for Quantum Science and Engineering, Southern University of Science and Technology, Shenzhen 518055, China*

[2] *International Quantum Academy, Shenzhen 518055, China*

[3] *Guangdong Provincial Key Laboratory of Quantum Science and Engineering, Southern University of Science and Technology, Shenzhen 518055, China*

[4] *Center for Quantum Technology Research, and Key Laboratory of Advanced Optoelectronic Quantum Architecture and Measurements, School of Physics, Beijing Institute of Technology, Beijing 100081, China*

(Received 14 June 2022; accepted 31 October 2022; published 23 November 2022)

High-fidelity control of quantum systems is crucial for quantum information processing, but is often limited by perturbations from the environment and imperfections in the applied control fields. Here, we investigate the combination of dynamical decoupling (DD) and robust optimal control (ROC) to address this problem. In this combination, ROC is employed to find robust shaped pulses, wherein the directional derivatives of the controlled dynamics with respect to control errors are reduced to a desired order. Then, we incorporate ROC pulses into DD sequences, achieving a remarkable improvement of robustness against multiple error channels. We demonstrate this method in the example of manipulating nuclear spin bath via an electron spin in the nitrogen-vacancy center system. Simulation results indicate that ROC-based DD sequences outperform the state-of-the-art robust DD sequences. Our work has implications for robust quantum control on near-term noisy quantum devices.

DOI: 10.1103/PhysRevApplied.18.054075

I. INTRODUCTION

Dynamical decoupling (DD) is a well-established open-loop quantum control technique [1] that has substantial applications, such as protecting quantum coherence [2–6], implementing high-fidelity quantum gates [7–10], probing noise spectrum [11,12], and quantum sensing [13–15]. In its basic form, a DD sequence comprises a series of instantaneous pulses on the system of concern, separated by certain interpulse delays. However, actual pulses must have bounded strengths and hence cannot be really instantaneous. Besides, there are inevitable pulse control imperfections, including off-resonant errors and control field fluctuations. These nonideal factors can cause a DD scheme fail to achieve the expected performance [16]. To overcome this problem, a commonly used approach is to apply pulses along different spatial directions to let the error of one pulse be compensated by other pulses [17–19]. Also, one can combine DD with composite pulses (CPs), which are robust against operational errors [20]. These efforts have yielded in the past decades a significant number of robust DD sequences, such as the XY8 [17], CDD [21], KDD [22], UR [23], and random-phase [24] sequences. However, since fighting against noise effects on current noisy intermediate-scale quantum [25] devices remains a compelling challenge, robust DD continues to be a significant research problem of strong interest.

Generally, for establishing a well-behaved robust DD sequence, several issues are particularly worth considering [1,16]. First, a satisfactory control fitness profile against imperfections resembles that shown in Fig. 1(a), i.e., the central robust region should be as broad and flat as possible. Second, it is desirable that the DD sequence can resist several types of imperfections simultaneously. This is a natural requirement because in realistic situations various perturbations exist concurrently. Third, the widths of the basic pulses need to be much shorter than the interpulse delays. However, present DD sequences usually do not meet all of these requirements. Take CP-based DD as an example, representative CPs like CORPSE [26] or BB1 [27] correct only a single error type, and concatenated CPs can correct simultaneously existing errors but only at the price of larger pulse widths [28], hence the CP technique does not easily lend itself to incorporating the desired robustness features.

In this work, we show that combining DD with robust optimal control (ROC) provides a general and effective

*bozhang_quantum@bit.edu.cn

†lij3@sustech.edu.cn

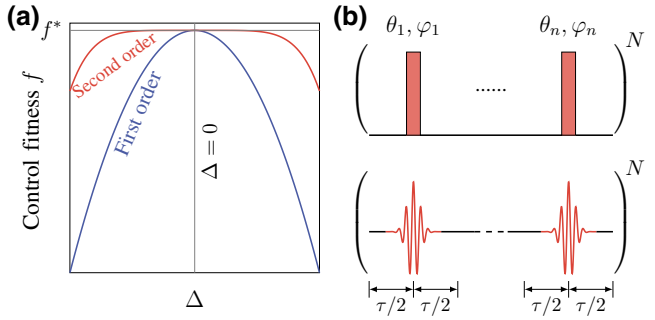

FIG. 1. (a) Robustness against pulse imperfection. The higher the level to which the derivatives of the fitness function with respect to the imperfections are reduced, the better. (b) Typical DD sequence structure combining a series of basic pulses with arbitrary shapes.

way to enhance robustness for multiple pulse errors. Here, ROC is in essence quantum optimal control [29] with the additional robustness constraint requiring that the leading-order effects of the imperfections are minimized. Our basic idea is to replace the hard pulses in DD with robust shaped pulses that are optimized via ROC algorithms [30]. The whole DD sequence is able to exhibit much improved error tolerance. As a demonstration, we apply this framework to the problem of manipulating a spin network via a single spin. In defect-based systems, such as nitrogen-vacancy (N-V) center in diamond [13,31,32] and silicon-based quantum dots [33,34], a frequently encountered control scenario is to use a single probe spin to explore properties of a quantum spin network in the proximity. This central spin can function as a polarizer, detector, or actuator [35,36], often resorting to the DD technique. Here, in particular, we focus on the task of nuclear spin detection and hyperpolarization by driving the electron spin only. Our numerical simulations show that ROC-based DD sequences outperform the other DD sequences available so far.

II. ROBUST DD

Consider a single spin as the system S coupled to a spin network as its interacting environment E. In the resonantly rotating frame of S, the free evolution Hamiltonian is $H = H_{SE} + H_E$. In DD, control is acted on S alone, which is implemented by a transversely applied time-dependent field $u(t) = (u_x(t), u_y(t))$. Let $S_\alpha = \sigma_\alpha/2$ $(\alpha = x, y, z)$, σ_α being the Pauli operators, then the control Hamiltonian is $H_C(u(t)) = u_x(t)S_x + u_y(t)S_y$. We assume the hierarchy in the coupling strengths, $H_C \gg H_{SE} \gg H_E$. As such, we can just omit the weak term H_E as it does not appear in the DD problem to the lowest order [37]. The general goal of DD is to find a suitable control sequence to synthesize a target effective dynamics of interest. However, in the actual implementation, DD must take into account control imperfections, as realistic pulse profiles inevitably incorporate pulse-shaping errors due to finite-power and finite-bandwidth constraints in hardware. Here, we view these imperfections as perturbations and write the perturbed Hamiltonian as

$$H(t) = H_{SE} + H_C(u(t)) + \sum_i \epsilon_i V_i(t), \tag{1}$$

in which $\{V_i(t)\}$ are noise operators, and $\{\epsilon_i\}$ are their corresponding weights. Specifically, we consider in this work mainly off-resonant and control amplitude errors, i.e., $V_1 = \Delta_{\max} S_z$ and $V_2(t) = H_C(u(t))$, where $\Delta_{\max}$ represents the maximum detuning. We note that this semiclassical model for describing pulse imperfections has been commonly used in many robust DD studies [22–24]. Our goal is to devise a robust DD protocol that realizes a given control target with sufficiently high accuracy for a broad range of noise strengths.

We start from a typical DD sequence of the structure shown in Fig. 1(b). The sequence is built based on a set of basic pulses $\{u_{\theta,0}(t) : 0 \le \theta \le \pi\}$, here $u_{\theta,0}(t)$ represents a control pulse intended to effect a single-qubit rotation $R_0(\theta)$ with angle θ and phase $\phi = 0$. More specifically, the sequence consists of sequentially combining n pulses from the basic pulse set, each with a phase shift, into a DD block, and then repeating this block for N times. The kth pulse in the DD block is denoted as $u_k = u_{\theta_k,\phi_k}$, obtained from $u_{\theta_k,0}$ by a phase shift ϕ_k. Adjacent pulses are time separated by τ, and we assume that for each pulse u_{θ_k,ϕ_k}, its pulse width τ_{u_k} is small compared with τ.

We want to quantify the control robustness of the considered DD sequence. First let us look into the errors that arise in applying a single pulse $u_{\theta,\phi}$. The real controlled time-evolution operator in the presence of perturbations is approximately $e^{-iH_{SE}\tau_u/2} U_{\theta,\phi} e^{-iH_{SE}\tau_u/2}$ with $U_{\theta,\phi} = \mathcal{T} e^{-i\int_0^{\tau_u} dt(H_C(t)+\epsilon_1 V_1+\epsilon_2 V_2(t))}$, where we allow only for the first-order effect of H_{SE} during the short period of pulse control. The H_{SE} evolutions can be incorporated into the free-evolution operators, so they evolve for the right amount of time. According to the Dyson perturbative theory [38], $U_{\theta,\phi}$ can be expanded as the series

$$U_{\theta,\phi} = R_\phi(\theta) + \sum_{i_1} \epsilon_{i_1} \mathcal{D}^{(1)}_{U_{\theta,\phi}}(V_{i_1}) + \sum_{i_1,i_2} \epsilon_{i_1}\epsilon_{i_2} \mathcal{D}^{(2)}_{U_{\theta,\phi}}(V_{i_1}, V_{i_2}) + \cdots, \tag{2}$$

in which the mth- $(m \ge 1)$ order terms $\mathcal{D}^{(m)}_{U_{\theta,\phi}}(V_{i_1}, \ldots, V_{i_m}) = (-i)^m R_\phi(\theta) \int_0^{\tau_u} dt_1 \cdots \int_0^{t_{m-1}} dt_m \widetilde{V}_{i_1}(t_1) \cdots \widetilde{V}_{i_m}(t_m)$ for $i_1, \ldots, i_m = 1, 2$ are referred to as the mth-order directional derivatives [30], characterizing the perturbative effects due to the noise generators $\{V_i\}$. Here, $\widetilde{V}_i(t) = U_C^\dagger(t) V_i(t) U_C(t)$

with $U_C(t) = \mathcal{T} e^{-i\int_0^t ds H_C(s)}$. Noting that $H_C(u_{\theta,\phi}(t)) = e^{-i\phi S_z} H_C(u_{\theta,0}(t)) e^{i\phi S_z}$, thus for any m and for any time-ordered operators $V_{i_1}, \ldots, V_{i_m}$, we can derive that

$$\mathcal{D}^{(m)}_{U_{\theta,\phi}} = e^{-i\phi S_z} \mathcal{D}^{(m)}_{U_{\theta,0}} e^{i\phi S_z}. \tag{3}$$

Thus there is $\left\| \mathcal{D}^{(m)}_{U_{\theta,\phi}} \right\|^2 = \left\| \mathcal{D}^{(m)}_{U_{\theta,0}} \right\|^2$, implying that we need only to consider the robustness of the basic pulses.

Now, for the whole DD block, the real propagator goes

$$U_{\mathrm{DD}} = W_n U_{\theta_n,\phi_n} W_n \cdots W_1 U_{\theta_1,\phi_1} W_1, \tag{4}$$

where $W_k = e^{-i(H_{SE}\tau/2 + \epsilon_1 V_1(\tau - \tau_{u_k})/2)}$ is the free-evolution operator, which has incorporated the H_{SE} evolution. It is then clear that the errors in U_{DD} in Eq. (4) include detuning errors in W_k as well as both detuning and control amplitude errors in U_{θ_k,ϕ_k}, up to first-order approximation with respect to H_{SE}. Hence, there are two feasible approaches toward robust DD. On the one hand, DD seeks to use a properly designed phase modulation strategy so that the errors will cancel rather than accumulate. Notable examples include the two-axis XY family [17], the multiaxis UR [23], and the random-phase [24] or correlated-random-phase [39] sequences. On the other hand, by minimizing the magnitudes of the directional derivatives $\mathcal{D}^{(m)}_{U_{\theta_k,0}}$, the robustness of the pulses $u_{\theta_k,\phi_k}(t)$ are enhanced, and the total error of the full sequence will be accordingly decreased. Furthermore, if both approaches are taken simultaneously, we anticipate that the DD robustness property will get improved to an even larger degree.

A particularly effective approach for devising shaped pulses that are robust to several simultaneously existing perturbations is the ROC algorithm developed in Ref. [30]. In our subsequent numerical simulations, we generally follow this approach. Basically, we attempt to solve the following multiobjective optimization problem: for a given target rotation angle θ, to optimize the shape of the pulse $u = u_{\theta,0}(t)$ to (i) maximize the fidelity between the unperturbed propagator and the target rotation $R_0^\dagger(\theta)$, and meanwhile (ii) minimize $\left\| \mathcal{D}^{(m)}_{U_{\theta_k,0}} \right\|^2$ for m up to a certain order. It is worth noting that the directional derivatives can be effectively calculated by the Van Loan block differential equation formalism [30]; see Appendix for details. One can employ either the known gradient-ascent pulse-engineering algorithm [40] or gradient-free methods like the differential evolution [41–43] algorithm to perform the pulse search. Note that in the entire space of admissible control functions, there may exist plenty of solutions that can accomplish the same control goal. However, as a realistic pulse generator has limited bandwidth, we exclude consideration of abruptly changing pulse shapes.

Now, we present some initial test results. In Fig. 2 we show a typical result of robust pulse that we obtain for realizing a π-rotational gate. It can be seen that our ROC pulse has stronger robustness compared with the SQUARE pulse and the composite pulses, including CORPSE and BB1. Meanwhile, the ROC pulse shape is smoother, which is favorable for experimental applications. We then put our ROC pulse into DD and examine the robustness of the whole sequence. Ideally, the overall effect of each DD sequence is an identity operation. In reality, the inevitable pulse imperfections will introduce errors that may accumulate during cycles of DD implementations. As described above, to reduce this side effect, one can resort to a properly designed phase-modulation strategy or robust basic pulse. Here, we incorporate different basic pulses into the XY8 and the UR8 [23] sequences to illustrate this point, as

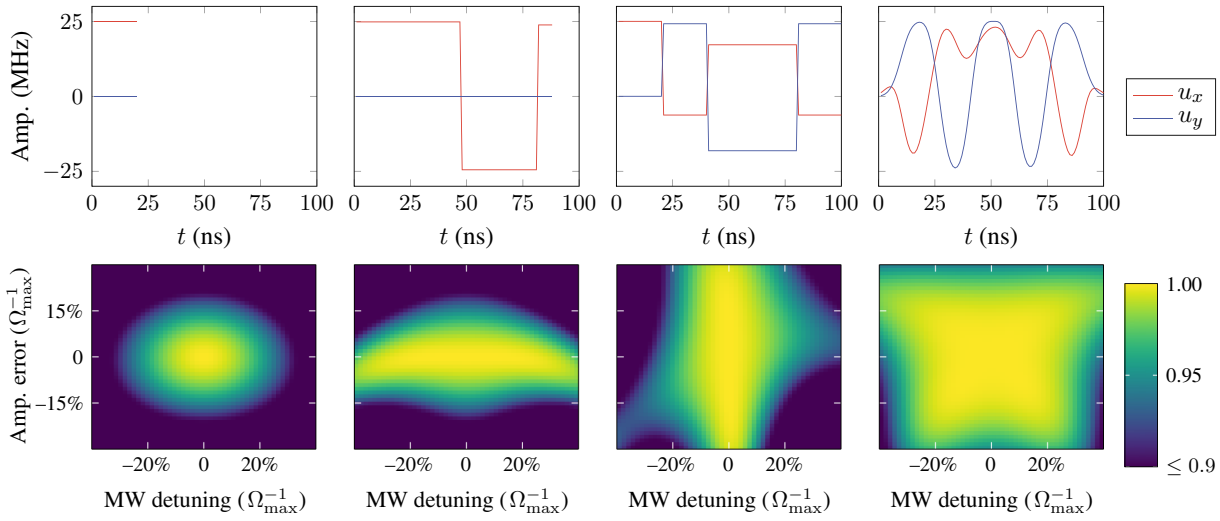

FIG. 2. Comparison of pulse shapes and robustness profiles for realizing a π-rotational gate $R_0(\pi)$ under pulse amplitude error and microwave (MW) detuning error. From left to right, the tested pulses are SQUARE, CORPSE, BB1, and ROC, respectively.

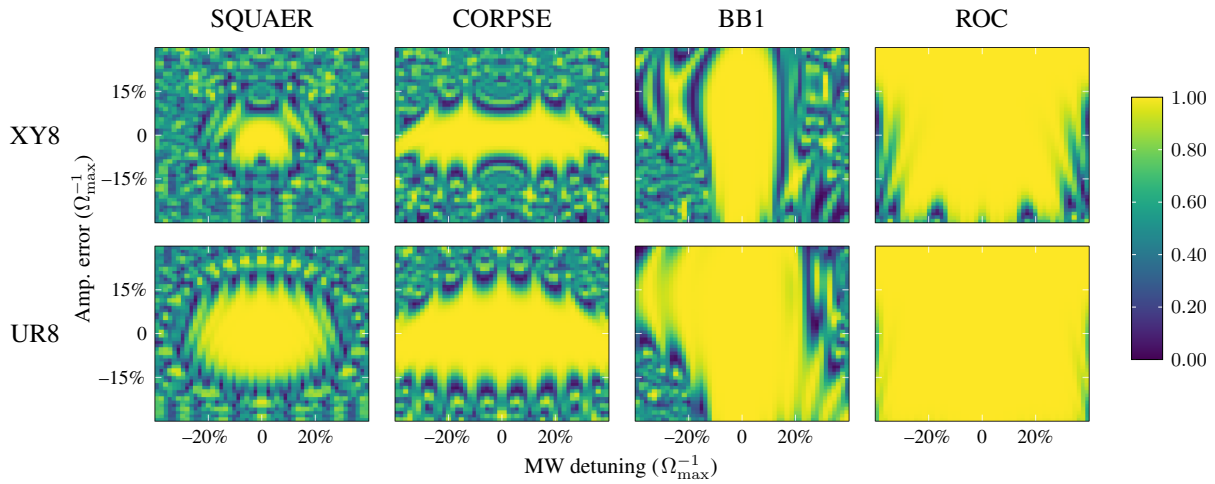

FIG. 3. Fidelity of XY8 and UR8 as an identity operation under pulse detuning and amplitude errors. The DD sequences employ different basic pulses, including SQUARE, CORPSE, BB1, and our ROC. Here, the control errors are measured in terms of the maximum Rabi frequency Ω_{max}. All DD sequences contain $N = 100$ cycles and have equal total time length of 3.2 ms.

shown in Fig. 3. We find that for the same basic pulse, UR8 outperforms XY8. This reveals that the phase-modulation strategy of UR8 is more robust, as expected in Ref. [23]. Then, fix the same phase-modulation strategy, our ROC pulse performs even better. This indicates that the designed ROC pulse is particularly effective for resisting the considered pulse imperfections for robust DD. In the next section, we study the applications of our optimized robust DD sequences.

III. APPLICATIONS

A. Robust detection of nuclear spins

Consider the system of an electron spin S ($S = 1/2$) of an N-V center in diamond and surrounding nuclear spins I ($I = 1/2$). The system is under a static magnetic field applied along the N-V axis, which is, by convention, defined as the $\hat{z}$ axis. The electron spin is subject to intermediately applied microwave control field $u(t)$. In a rotating frame with respect to $\Omega_S S_z$, the Hamiltonian after the secular approximation reads

$$H = \sum_j \Omega_I I_z^j + \sum_j S_z (A_{zz}^j I_z^j + A_{zx}^j I_x^j) + H_C(u(t)),$$

in which Ω_S (Ω_I) denotes the electron (nuclear) Larmor frequency, A_{zz} and A_{zx} are the hyperfine coupling strengths. In our numerical studies, we assume the existence of a minimum switching time $t_{min} = 1$ ns for pulse modulation and require all control amplitudes to be bounded by $\Omega_{max} = 2\pi \times 25$ MHz. Three common pulse imperfections, namely detuning, control amplitude error, and finite pulse width, are under consideration.

First, we investigate the detection of nuclear spins via the central electron spin. Nuclear spins exist naturally in abundance in N-V center systems, providing possible additional quantum resources [15,44,45]. A prerequisite to exploit this potential is to detect and characterize them, usually with the aid of the electron spin. Ideally, the jth nuclear spin with the effective Larmor frequency $\omega_I^j = \Omega_I + A_{zz}^j/2$ can induce a sharp electron signal in the observed spectrum, by applying a multipulse DD sequence on the electron spin with the interpulse delay $\tau = k\pi/\omega_I^j$ (k is odd) [13]. Nevertheless, addressing and controlling nuclear spins is challenging as the spins are generally embedded in noisy spin bath, and the inevitable pulse imperfections can induce spurious peaks [46] and distortion of the spectrum [47]. To avoid false identification, many robust DD sequences were proposed [22–24,47,48]. However, when the pulse imperfections are relatively large and exist simultaneously, we find that the performance of the present robust DD sequences can be further improved by using ROC pulses.

As an initial demonstration, let us consider the situation of detecting a single ^{13}C nuclear spin. The simulated spectra with using four representative robust DD sequences are shown in Fig. 4(a). For conventional XY8 sequence, there exist miscellaneous errors in the signal, including the tilted baseline that causes severely reduced contrast, the phase-distorted resonant peaks, and the spurious peaks appearing due to finite pulse width and detuning effects [46], so the spectrum is hard to analyze and identify. Substituting the square-shaped π pulses with BB1 in XY8 (BB1-XY8) [27], or using the UR8 sequence [23], improves the signal, but still does not solve the spurious peak problem. A recently proposed random-phase XY8 (RP-XY8) sequence [24] can largely suppress the spurious peaks and maintain the signal contrast, but still induce dense small miscellaneous peaks near the baseline. It is

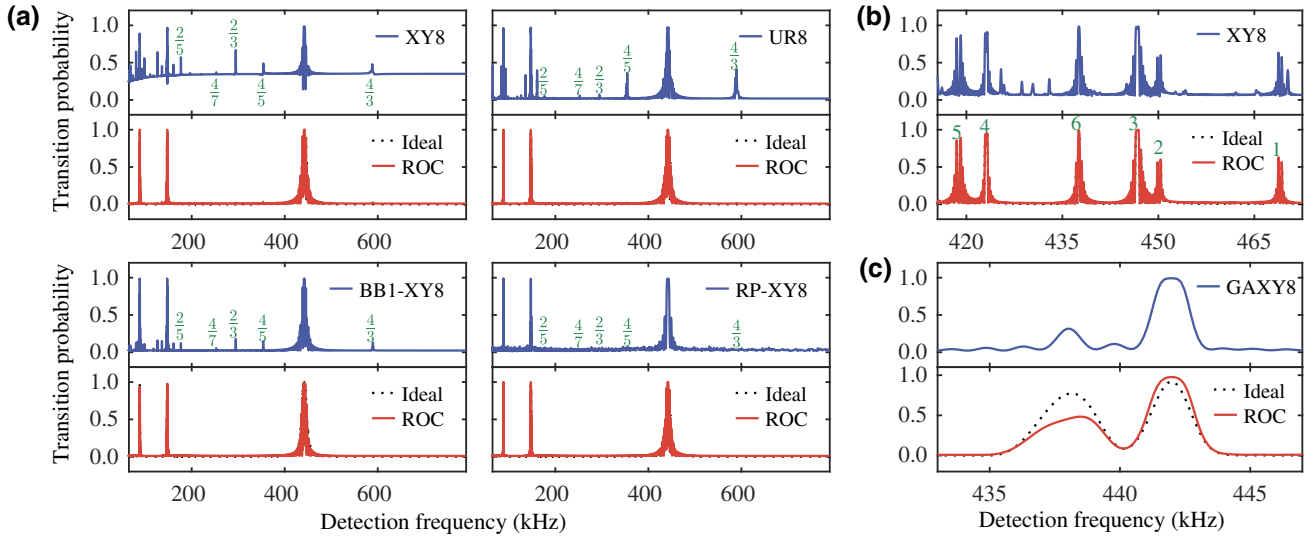

FIG. 4. Simulated spectra of detecting nuclear spins, where the control imperfection parameters are set as detuning $8\% \times \Omega_{\max}$, amplitude error $8\% \times \Omega_{\max}$, and π pulse with a limit width $1/(2\Omega_{\max}) = 20$ ns. The number of cycles for (a), (b), and (c) are 96, 32, and 64, respectively. (a) Signal from a single spin with $\omega_I = 2\pi \times 441.91$ kHz detected by various DD sequences. The results for XY8, UR8, BB1-XY8, RP-XY8, and their ROC counterparts are presented. Clearly, using our ROC pulses excellently solves the baseline distortion problem and eliminates the spurious peaks (green marker) that are located at $2\omega_I/k$ and $4\omega_I/k$ (k is odd) [46]. (b) Signal from six spins (see simulation parameters in the Appendix). The miscellaneous peaks appeared in applying XY8 greatly hamper the identification of each spin, but can be circumvented by ROC-XY8. (c) Signal from two spectrally close spins with $\omega_I^1 = 2\pi \times 441.91$ kHz and $\omega_I^2 = 2\pi \times 437.53$ kHz. It can be seen that, the ROC-based sequence shows better robustness against imperfections in resolving the two spins.

found that, for all these sequences, if implemented with our ROC pulses ($t_{\mathrm{ROP}} = 80$ ns), then the errors almost disappear, giving a rather clean spectrum close to the ideal one.

Next, we consider detecting multiple ^{13}C nuclear spins. The case of six nuclear spins is presented in Fig. 4(b). As can be seen from the spectrum, a bunch of spurious peaks exist, making it a difficult task to identify the spins. This gets even worse when the cycle number N is large. Again, combining XY8 with our ROC pulses suppresses all the unwanted peaks to a satisfactory extent. As an additional demonstration example, we consider the problem of detecting two spectrally close nuclear spins. This situation demands good selectivity of the control sequence in addressing the nuclear spins individually. Recently, Ref. [49] proposed an effective soft temporal modulation sequence named Gaussian AXY8, which has better selectivity than conventional XY8. However, when taking into account pulse imperfections, distortions occur in the transition probabilities of the spins, leading to off-resonant side peaks and hence reducing the signal contrast, as shown in Fig. 4(c). We thus test with our ROC pulses, finding that the side peaks around the spin resonances are all removed, and consequently the two spins are well resolved. Clearly, our approach is of great benefit when fitting dense signals for many close nuclear spins, especially when spurious resonances exist.

B. Robust dynamical nuclear polarization of the nuclear spins

Now, we turn to the application to dynamical nuclear polarization (DNP) of the nuclear spins. DNP aims to transfer the almost perfect polarization of the optically initialized electron spin to its surrounding nuclear spins; see Fig. 5(a). This could result in an enhancement of the nuclear signal by several orders of magnitude, which is crucial for a variety of quantum technologies, such as magnetic resonance imaging [50]. The goal of achieving high-efficiency DNP in N-V centers in diamond has attracted a lot of interests in recent years but remains technically challenging. Key factors affecting effective polarization, include the large spectral random orientation of the N-V center axes and Rabi power imperfection. For example, conventionally DNP uses the Hartmann-Hahn resonance [51], the corresponding NOVEL sequence [52] works only in a narrow frequency range. Hence, there have been efforts made in devising more robust DNP protocols [51,53,54]. A significant advance was made by Ref. [55], which put forward a Hamiltonian engineering-based approach termed PulsePol, featuring both fast polarization and excellent robustness. Yet, we find that the results presented in Ref. [55] can still be improved, with using our ROC-shaped pulses.

For simplicity, we consider a single electron coupled to a single nuclear spin. The PulsePol sequence, as shown in

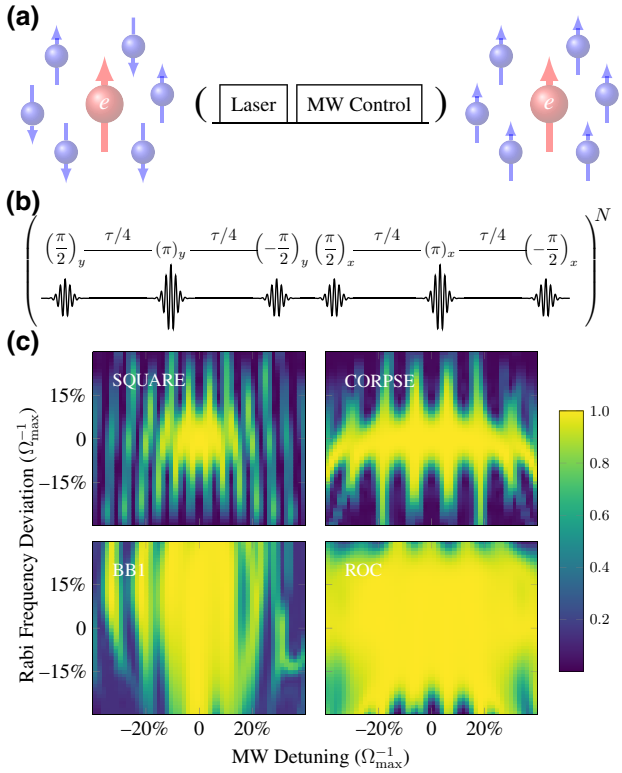

FIG. 5. (a) Schematics of the MW pulse sequence on the electron spin for pulsed polarization transfer to the surrounding nuclear spins. (b) The PulsePol sequence. As stated, the pulse duration should not take a large fraction of the free-evolution time. (c) Comparison of error resistance of four different PulsePol sequences.

Fig. 5(b), consists of N cycles each with four $\pi/2$ pulses and two π pulses, and operates for a choice of pulse spacing $\tau = l\pi/\omega_I$ for odd l. Ideally, it produces an effective flip-flop Hamiltonian as $H_{\text{eff}} = \alpha A_{zx}(S_+I_- + S_-I_+)$, where $S_\pm = S_x \pm iS_y$, $I_\pm = I_x \pm iI_y$. As such, full polarization transfer is achieved at time $2N\tau = 1/(\alpha A_{zx})$. However, because real pulses take a finite time, the free evolutions between the pulses need be adjusted according to $\tau_{\text{free}} = \tau - 4t_{\pi/2} - 2t_\pi$, where $t_{\pi/2}$ and t_π denote the time length of the $\pi/2$ and π pulses. As a consequence, the number of cycles N required for full polarization transfer varies depending on the specific pulses used. In our simulations, we compare the robustness performance achieved from using four different realizations of the rotations, namely squared, CORPSE, BB1, and our ROC pulses. The simulations are implemented with the coupling strength $A_{zx} = 0.03$ MHz, the resonance $l = 5$, and the same cycle number $N = 29$. The results are shown in Fig. 5(c). First, we clearly see that the robustness of PulsePol for using rectangular pulses is the worst. Then, the performance can be improved against detuning errors for CORPSE or against Rabi frequency errors for BB1. Finally, the best results are achieved with our ROC pulses. There is a rather large flat central area of the robustness profile: the flat region satisfying $f \geq 0.99$ covers the entire error range of ± 5 MHz detuning and $\pm 10\%$ Rabi frequency deviation.

IV. CONCLUSION

We present a flexible and effective framework for integrating DD with ROC. Unlike hard pulses, shaped pulses produced by ROC with smooth constraints are friendly to hardware implementation. In principle, ROC pulses can be incorporated into any DD sequence for robustness improvement. This is confirmed in our test examples of nuclear spin-bath detection and hyperpolarization on N-V center systems. Our method is ready to be exploited in many other spin-network-related problems, such as creating collective quantum memory [56], probing thermalization [57], exploring condensed-matter phenomena [58], and studying magnetic dynamics of nanoparticles [59]. ROC-based DD sequences can resist multiple errors simultaneously. This is especially useful for near-term noisy quantum devices. For instance, recent benchmark experiments in superconducting qubits have identified real coexisting error channels as well as their respective contribution [60,61], which are to be compensated for realization of high-fidelity quantum computing. Therefore, a meaningful extension of the current work is to explore how to achieve the best robustness given knowledge of error channels and their weights. Lastly and of note, future research could explore alternative ROC strategies that can deal with time-dependent perturbations, which is a key ingredient to allowing robust DD to find a broader range of application scenarios [62,63].

ACKNOWLEDGMENTS

This work is supported by the National Natural Science Foundation of China (Grants No. 1212200199, No. 12204230, No. 11975117, No. 92065111, and No. 12004037), China Postdoctoral Science Foundation (2021M691445), Guangdong Basic and Applied Basic Research Foundation (Grant No. 2021B1515020070), Guangdong Provincial Key Laboratory (Grant No. 2019B121203002), and Shenzhen Science and Technology Program (Grants No. RCYX2020071411452210 9 and No. KQTD20200820113
010023).

APPENDIX A: VAN LOAN BLOCK DIFFERENTIAL EQUATION FORMALISM

In our applications, we denote the pulse detuning error and amplitude error as $V_1 = \Delta_{\max} S_z$ and $V_2 = H_C(u(t))$, respectively. A typical DD sequence consists of a series of π-rotational pulses with different phases. According to our analysis, we need only to search a robust π-rotational pulse with phase 0. For simplicity, we denote

$U_C \equiv U_{\theta_k,0}$. To effectively calculate the directional derivatives $\mathcal{D}^{(m)}_{U_C}(V_{i_1},\ldots V_{i_m})$, we follow the method in Ref. [30]. As an example, we show how to compute the first- and second-order directional derivatives. Concretely, the Van Loan block differential equations are constructed as follows ($i_1, i_2 = 1$ or 2):

$$\dot{V}(t) = -i \begin{pmatrix} H_C(t) & V_{i_1}(t) & 0 \\ 0 & H_C(t) & V_{i_2}(t) \\ 0 & 0 & H_C(t) \end{pmatrix} V(t).$$

Its time-evolution solution is, according to the Van Loan integral formula, given by

$$V(\tau_u) = \mathcal{T} \exp\left[-i \int_0^{\tau_u} dt \begin{pmatrix} H_C(t) & V_{i_1}(t) & 0 \\ 0 & H_C(t) & V_{i_2}(t) \\ 0 & 0 & H_C(t) \end{pmatrix} \right] = \begin{pmatrix} U_C(\tau_u) & \mathcal{D}^{(1)}_{U_C}(V_{i_1}) & \mathcal{D}^{(2)}_{U_C}(V_{i_1}, V_{i_2}) \\ 0 & U_C(\tau_u) & \mathcal{D}^{(1)}_{U_C}(V_{i_2}) \\ 0 & 0 & U_C(\tau_u) \end{pmatrix}.$$

From this solution, the first- and second-order directional derivatives can then be directly extracted. The higher-order directional derivatives can also be computed in a similar way.

APPENDIX B: GRADIENT-BASED ALGORITHM

We describe how the gradient-based algorithm works for searching ROC pulse. To maximize the fidelity and minimize the magnitudes of the directional derivatives, we define a fitness function

$$\Phi(u) = \left| \mathrm{Tr}\left(U_C(\tau_u) R_0^\dagger(\theta) \right) \right|^2 - \sum_{m=1}^{m_{\max}} \sum_{i_1,\ldots,i_m=1}^{2} \mu^{(m)}_{i_1,\ldots,i_m} \left\| \mathcal{D}^{(m)}_{U_C}(V_{i_1},\ldots V_{i_m}) \right\|^2,$$

in which $m_{\max}$ is the maximum order of directional derivatives involved, $\mu^{(m)}_{i_1,\ldots,i_m} > 0$ are a set of weights specifying the relevance of the associated objective function and are often adjusted during optimization.

The gradient ascent pulse-engineering (GRAPE) algorithm proposed in Ref. [40] is a standard gradient-based numerical method for solving quantum optimal control problems. GRAPE works as follows:

(1) start from an initial pulse guess $u[l]$, $l = 1,\ldots,L$;
(2) compute the gradient of the fitness function with respect to the pulse parameters $\partial\Phi/\partial u[l]$;
(3) determine a gradient-related search direction $p[l]$, $l = 1,\ldots,L$;
(4) determine an appropriate step length α along the search direction p;
(5) update the pulse parameters: $u[l] \leftarrow u[l] + \alpha \times p[l]$;
(6) if Φ is sufficiently high, terminate; else, go to step 2.

APPENDIX C: BASIC PRINCIPLES AND SEQUENCE PARAMETERS FOR SPIN DETECTION

In the N-V center system, through applying a subtle multipulse DD sequence on the electron spin, the weak signal of a specific nuclear spin can be amplified, meanwhile all the other nuclear spins can be dynamically decoupled from the central electron spin. As such, we can resolve and coherently control the nuclear spins. Specifically, the electron spin is firstly prepared at $\rho = |+\rangle\langle+|$ with $|+\rangle = (|0\rangle + |1\rangle)/\sqrt{2}$ and a DD sequence then follows. Finally, the resultant electron spin state ρ_t is attached to a $R_{\pi/2}(\pi/2)$ rotation and measured in the basis $|0\rangle$, thus we can obtain the transition probability $P = \mathrm{Tr}(\rho_f\,|0\rangle\langle 0|)$. We use $R_{\phi_k}(\theta)$ to represent a θ rotation around the axis $S_{\phi_k} = \cos(\phi_k)S_x + \sin(\phi_k)S_y$.

When the interpulse delay $\tau = k\pi/\omega_I$ (k is odd number), the corresponding nuclear spin with effective Larmor frequency ω_I can induce a sharp resonant dip in the observed signal (time domain) [13]. This basic unit is usually cycled L times to enhance the signal. The position and amplitude of the dip are then used to infer the hyperfine couplings between the electron spin and the sensed nuclear spin. Equivalently, we can transform this signal to frequency domain, i.e., a sharp resonant peak with detection frequency $\omega = \omega_I/k$, for clearly acquiring the spectrum information. In the realistic case, many common pulse imperfections can severely hinder the detection process. Finite width of the π pulses, marked as t_π, will shift the resonant positions to $\tau' = k\pi/\omega_I - t_\pi/2$. Detuning and pulse amplitude error can cause spurious peaks and distortion of the baseline. Thus, robust DD sequences that can resist these pulse imperfections are highly in demand. In this work, we consider the following representative DD sequences ($\Omega_{\max} = 25$ MHz).

(1) XY8 sequence. The phases of the basic pulses are $\phi_k^{\mathrm{XY8}} = \{0,\pi/2,0,\pi/2,\pi/2,0,\pi/2,0\}$. The resonant positions are $\tau' = k\pi/\omega_I - t_\pi/2$ with $t_\pi = 20$ ns.
(2) UR8 sequence. The phases of the basic pulses are $\phi_k^{\mathrm{UR8}} = \{0,\pi/2,3\pi/2,\pi,\pi,3\pi/2,\pi/2,0\}$. The resonant positions are $\tau' = k\pi/\omega_I - t_\pi/2$ with $t_\pi = 20$ ns.
(3) BB1-XY8 sequence. The phases of the basic pulses are $\phi_k^{\text{BB1-XY8}} = \{0,\pi/2,0,\pi/2,\pi/2,0,\pi/2,0\}$. Each $R_{\phi_k}(\pi)$ is realized by the BB1 composite pulses, namely $R_{\phi_k}(\pi) = \Pi_{i=1}^4 R_{\phi_i}(\theta_i)$ with $\theta_1 = \theta_3 = \pi, \theta_2 = 2\pi$, $\theta_4 = \pi; \phi_1 = \phi_3 = \phi_k + \arccos(-1/4), \phi_2 = 3\phi_1 - 2\phi_k$, $\phi_4 = \phi_k$. The resonant positions then become $\tau' = k\pi/\omega_I - t_{\mathrm{BB1}}/2$ with $t_{\mathrm{BB1}} = 5t_\pi = 100$ ns.

(4) RP-XY8 sequence [24]. The phases of the basic pulses are $\phi_k^{\text{RP-XY8}} = \phi_k^{\text{XY8}} + \phi_n, \phi_n \in \text{rand}[0, 2\pi], n = 1, 2, \ldots, N$. That is, the eight basic pulses in each unit are attached to a random global phase. The resonant positions are $\tau' = k\pi/\omega_I - t_\pi/2$ with $t_\pi = 20$ ns.

(5) GAXY8 sequence [49]. The phases of the basic pulses are $\phi_k^{\text{GAXY8}} = \{0, \pi/2, 0, \pi/2, \pi/2, 0, \pi/2, 0\}$. Each basic π rotation is then realized by the five-pulse composite AXY8 sequence [47]. Further, each AXY8 sequence employs a different amplitude but keeps the same in a DD unit. In this way, the soft modulation can be resembled as the Gaussian shape $\lambda(t) = \lambda_0 \exp\left[-t^2/\left(2\sigma^2\right)\right]$ by the sequence of hard π pulses, we set $\sigma = T/(4\sqrt{2})$ with $\lambda_0 = 0.271, T = 4L\tau$. The resonant positions are $\tau' = k\pi/\omega_I - t_{\text{AXY8}}$ with $t_{\text{AXY8}} = 5t_\pi = 100$ ns.

APPENDIX D: SIMULATION DETAILS OF SPIN DETECTION

Here, we supplement some details of Fig. 4 in the main text.

1. Detection of a single nuclear spin

The hyperfine couplings and the effective Larmor frequency [Fig. 4(a) in the main text] are $A_{zz}^1 = 2\pi \times 27$ kHz, $A_{zx}^1 = 2\pi \times 17$ kHz, $\omega_I = 2\pi \times 428.41$ kHz. As analyzed, the kth-order resonant peak appears at the location ω_I/k with k being odd. For brevity, we show only the resonant peaks up to third order.

2. Detection of six nuclear spins

The detailed coupling constants between the N-V electron spin and the surrounding six nuclear spins [Fig. 4(b) in the main text] are listed in Table I. We show a spectrum range containing up to eighth-order resonant peaks of the six spins. It is worth noting that the spectrum will be hard to resolve with the XY8 sequence when the cycle number L becomes much larger, while our ROC-based DD leads to a relatively clean spectrum.

TABLE I. The hyperfine couplings and the effective Larmor frequency for the six nuclear spins used in our simulation; the data are from Ref. [13]. The Larmor frequency for each nuclear spin is $\Omega_I = \gamma_I B$ with $\gamma_I = 2\pi \times 1.071$ kHz/G and $B = 401$ G.

Spin	A_{zz}^n (kHz)	A_{zx}^n (kHz)	ω_I^n (kHz)
1	$2\pi \times 78.234$	$2\pi \times 30.031$	$2\pi \times 468.59$
2	$2\pi \times 40.703$	$2\pi \times 23.500$	$2\pi \times 449.82$
3	$2\pi \times 32.328$	$2\pi \times 44.496$	$2\pi \times 445.64$
4	$-2\pi \times 12.958$	$2\pi \times 13.896$	$2\pi \times 422.99$
5	$-2\pi \times 22.081$	$2\pi \times 24.525$	$2\pi \times 418.43$
6	$2\pi \times 15.796$	$2\pi \times 19.506$	$2\pi \times 437.37$

3. Detection of two close nuclear spins

In Fig. 4(c) in the main text, we use two spectrally close spins with couplings $A_{zz}^1 = 2\pi \times 27.02$ kHz, $A_{zx}^1 = 2\pi \times 16.91$ kHz, $\omega_I^1 = 2\pi \times 441.91$ kHz $A_{zz}^2 = 2\pi \times 18.28$ kHz, $A_{zx}^2 = 2\pi \times 54.26$ kHz, and $\omega_I^2 = 2\pi \times 437.53$ kHz. In our demonstrations, we minimize only the norm of the directional derivatives up to the second order. We anticipate that the visible gap between our results and the ideal spectra can be gradually bridged with higher-order minimizations of the directional derivatives.

[1] D. Suter and G. A. Álvarez, Colloquium: Protecting quantum information against environmental noise, Rev. Mod. Phys. **88**, 041001 (2016).

[2] L. Viola, E. Knill, and S. Lloyd, Dynamical Decoupling of Open Quantum Systems, Phys. Rev. Lett. **82**, 2417 (1999).

[3] J. Du, X. Rong, N. Zhao, Y. Wang, J. Yang, and R. B. Liu, Preserving electron spin coherence in solids by optimal dynamical decoupling, Nautre **461**, 1265 (2009).

[4] M. J. Biercuk, H. Uys, A. P. VanDevender, N. Shiga, W. M. Itano, and J. J. Bollinger, Optimized dynamical decoupling in a model quantum memory, Nautre **458**, 996 (2009).

[5] G. de Lange, Z. H. Wang, D. Ristè, V. V. Dobrovitski, and R. Hanson, Universal dynamical decoupling of a single solid-state spin from a spin bath, Science **330**, 60 (2010).

[6] M. Zhong, M. P. Hedges, R. L. Ahlefeldt, J. G. Bartholomew, S. E. Beavan, S. M. Wittig, J. J. Longdell, and M. J. Sellars, Optically addressable nuclear spins in a solid with a six-hour coherence time, Nature **517**, 177 (2015).

[7] J. R. West, D. A. Lidar, B. H. Fong, and M. F. Gyure, High Fidelity Quantum Gates via Dynamical Decoupling, Phys. Rev. Lett. **105**, 230503 (2010).

[8] G.-Q. Liu, H. C. Po, J. Du, R.-B. Liu, and X.-Y. Pan, Noise-resilient quantum evolution steered by dynamical decoupling, Nat. Commun. **4**, 2254 (2013).

[9] C. Piltz, B. Scharfenberger, A. Khromova, A. F. Varón, and C. Wunderlich, Protecting Conditional Quantum Gates by Robust Dynamical Decoupling, Phys. Rev. Lett. **110**, 200501 (2013).

[10] J. Zhang and D. Suter, Experimental Protection of Two-Qubit Quantum Gates against Environmental Noise by Dynamical Decoupling, Phys. Rev. Lett. **115**, 110502 (2015).

[11] J. Bylander, S. Gustavsson, F. Yan, F. Yoshihara, K. Harrabi, G. Fitch, D. G. Cory, Y. Nakamura, J.-S. Tsai, and W. D. Oliver, Noise spectroscopy through dynamical decoupling with a superconducting flux qubit, Nat. Phys. **7**, 565 (2011).

[12] G. A. Álvarez and D. Suter, Measuring the Spectrum of Colored Noise by Dynamical Decoupling, Phys. Rev. Lett. **107**, 230501 (2011).

[13] T. H. Taminiau, J. J. T. Wagenaar, T. van der Sar, F. Jelezko, V. V. Dobrovitski, and R. Hanson, Detection and Control of Individual Nuclear Spins Using a Weakly Coupled Electron Spin, Phys. Rev. Lett. **109**, 137602 (2012).

[14] J. E. Lang, R. B. Liu, and T. S. Monteiro, Dynamical-Decoupling-Based Quantum Sensing: Floquet Spectroscopy, Phys. Rev. X **5**, 041016 (2015).
[15] M. Abobeih, J. Randall, C. Bradley, H. Bartling, M. Bakker, M. Degen, M. Markham, D. Twitchen, and T. Taminiau, Atomic-scale imaging of a 27-nuclear-spin cluster using a quantum sensor, Nature **576**, 411 (2019).
[16] A. M. Souza, G. A. Álvarez, and D. Suter, Robust dynamical decoupling, Phil. Trans. R. Soc. A **370**, 4748 (2012).
[17] A. A. Maudsley, Modified Carr-Purcell-Meiboom-Gill sequence for NMR Fourier imaging applications, J. Magn. Reson. **69**, 488 (1986).
[18] L. Viola and E. Knill, Robust Dynamical Decoupling of Quantum Systems with Bounded Controls, Phys. Rev. Lett. **90**, 037901 (2003).
[19] K. Khodjasteh and L. Viola, Dynamically Error-Corrected Gates for Universal Quantum Computation, Phys. Rev. Lett. **102**, 080501 (2009).
[20] M. H. Levitt, Composite pulses, Prog. Nucl. Magn. Reson. Spectrosc. **18**, 61 (1986).
[21] K. Khodjasteh and D. A. Lidar, Fault-Tolerant Quantum Dynamical Decoupling, Phys. Rev. Lett. **95**, 180501 (2005).
[22] A. M. Souza, G. A. Álvarez, and D. Suter, Robust Dynamical Decoupling for Quantum Computing and Quantum Memory, Phys. Rev. Lett. **106**, 240501 (2011).
[23] G. T. Genov, D. Schraft, N. V. Vitanov, and T. Halfmann, Arbitrarily Accurate Pulse Sequences for Robust Dynamical Decoupling, Phys. Rev. Lett. **118**, 133202 (2017).
[24] Z.-Y. Wang, J. E. Lang, S. Schmitt, J. Lang, J. Casanova, L. McGuinness, T. S. Monteiro, F. Jelezko, and M. B. Plenio, Randomization of Pulse Phases for Unambiguous and Robust Quantum Sensing, Phys. Rev. Lett. **122**, 200403 (2019).
[25] J. Preskill, Quantum computing in the NISQ era and beyond, Quantum **2**, 79 (2018).
[26] H. K. Cummins, G. Llewellyn, and J. A. Jones, Tackling systematic errors in quantum logic gates with composite rotations, Phys. Rev. A **67**, 042308 (2003).
[27] S. Wimperis, Broadband, narrowband, and passband composite pulses for use in advanced NMR experiments, J. Magn. Reson. A **109**, 221 (1994).
[28] M. Bando, T. Ichikawa, Y. Kondo, and M. Nakahara, Concatenated composite pulses compensating simultaneous systematic errors, J. Phys. Soc. Jpn. **82**, 014004 (2013).
[29] J. Werschnik and E. K. U. Gross, Quantum optimal control theory, J. Phys. B: At. Mol. Opt. Phys. **40**, R175 (2007).
[30] H. Haas, D. Puzzuoli, F. Zhang, and D. G. Cory, Engineering effective Hamiltonians, New J. Phys. **21**, 103011 (2019).
[31] S. Kolkowitz, Q. P. Unterreithmeier, S. D. Bennett, and M. D. Lukin, Sensing Distant Nuclear Spins with a Single Electron Spin, Phys. Rev. Lett. **109**, 137601 (2012).
[32] P. London, J. Scheuer, J.-M. Cai, I. Schwarz, A. Retzker, M. B. Plenio, M. Katagiri, T. Teraji, S. Koizumi, J. Isoya, R. Fischer, L. P. McGuinness, B. Naydenov, and F. Jelezko, Detecting and Polarizing Nuclear Spins with Double Resonance on a Single Electron Spin, Phys. Rev. Lett. **111**, 067601 (2013).
[33] J. J. Pla, K. Y. Tan, J. P. Dehollain, W. H. Lim, J. J. Morton, D. N. Jamieson, A. S. Dzurak, and A. Morello, A single-atom electron spin qubit in silicon, Nature **489**, 541 (2012).
[34] J. J. Morton, A. M. Tyryshkin, R. M. Brown, S. Shankar, B. W. Lovett, A. Ardavan, T. Schenkel, E. E. Haller, J. W. Ager, and S. Lyon, Solid-state quantum memory using the ^{31}P nuclear spin, Nature **455**, 1085 (2008).
[35] L. Schlipf, T. Oeckinghaus, K. Xu, D. B. R. Dasari, A. Zappe, F. F. de Oliveira, B. Kern, M. Azarkh, M. Drescher, M. Ternes, K. Kern, J. Wrachtrup, and A. Finkler, A molecular quantum spin network controlled by a single qubit, Sci. Adv. **3**, e1701116 (2017).
[36] A. Ajoy, U. Bissbort, D. Poletti, and P. Cappellaro, Selective Decoupling and Hamiltonian Engineering in Dipolar Spin Networks, Phys. Rev. Lett. **122**, 013205 (2019).
[37] D. A. Lidar, E. Todd, and A. Brun, *Quantum Error Correction* (Cambridge University Press, Cambridge, England, 2013).
[38] F. J. Dyson, The radiation theories of Tomonaga, Schwinger, and Feynman, Phys. Rev. **75**, 486 (1949).
[39] Z. Wang, J. Casanova, and M. B. Plenio, Enhancing the robustness of dynamical decoupling sequences with correlated random phases, Symmetry **12**, 730 (2020).
[40] N. Khaneja, T. Reiss, C. Kehlet, T. Schulte-Herbrüggen, and S. J. Glaser, Optimal control of coupled spin dynamics: Design of NMR pulse sequences by gradient ascent algorithms, J. Magn. Reson. **172**, 296 (2005).
[41] P. Palittapongarnpim, P. Wittek, E. Zahedinejad, S. Vedaie, and B. C. Sanders, Learning in quantum control: High-dimensional global optimization for noisy quantum dynamics, Neurocomputing **268**, 116 (2017).
[42] D. Dong, X. Xing, H. Ma, C. Chen, Z. Liu, and H. Rabitz, Learning-based quantum robust control: Algorithm, applications, and experiments, IEEE Trans. Cybern. **50**, 3581 (2020).
[43] E. Zahedinejad, J. Ghosh, and B. C. Sanders, High-Fidelity Single-Shot Toffoli Gate via Quantum Control, Phys. Rev. Lett. **114**, 200502 (2015).
[44] T. D. Ladd, F. Jelezko, R. Laflamme, Y. Nakamura, C. Monroe, and J. L. O'Brien, Quantum computers, Nature **464**, 45 (2010).
[45] C. E. Bradley, J. Randall, M. H. Abobeih, R. C. Berrevoets, M. J. Degen, M. A. Bakker, M. Markham, D. J. Twitchen, and T. H. Taminiau, A Ten-Qubit Solid-State Spin Register with Quantum Memory up to One Minute, Phys. Rev. X **9**, 031045 (2019).
[46] M. Loretz, J. M. Boss, T. Rosskopf, H. J. Mamin, D. Rugar, and C. L. Degen, Spurious Harmonic Response of Multipulse Quantum Sensing Sequences, Phys. Rev. X **5**, 021009 (2015).
[47] J. Casanova, Z.-Y. Wang, J. F. Haase, and M. B. Plenio, Robust dynamical decoupling sequences for individual-nuclear-spin addressing, Phys. Rev. A **92**, 042304 (2015).
[48] J. Casanova, Z.-Y. Wang, and M. B. Plenio, Noise-Resilient Quantum Computing with a Nitrogen-Vacancy Center and Nuclear Spins, Phys. Rev. Lett. **117**, 130502 (2016).
[49] J. F. Haase, Z.-Y. Wang, J. Casanova, and M. B. Plenio, Soft Quantum Control for Highly Selective Interactions among Joint Quantum Systems, Phys. Rev. Lett. **121**, 050402 (2018).

[50] E. Rej, T. Gaebel, T. Boele, D. E. Waddington, and D. J. Reilly, Hyperpolarized nanodiamond with long spin-relaxation times, Nat. Commun. **6**, 8459 (2015).

[51] J. Scheuer, I. Schwartz, S. Müller, Q. Chen, I. Dhand, M. B. Plenio, B. Naydenov, and F. Jelezko, Robust techniques for polarization and detection of nuclear spin ensembles, Phys. Rev. B **96**, 174436 (2017).

[52] A. Henstra, P. Dirksen, J. Schmidt, and W. Wenckebach, Nuclear spin orientation via electron spin locking (NOVEL), J. Magn. Reson. **77**, 389 (1988).

[53] Q. Chen, I. Schwarz, F. Jelezko, A. Retzker, and M. B. Plenio, Optical hyperpolarization of ^{13}C nuclear spins in nanodiamond ensembles, Phys. Rev. B **92**, 184420 (2015).

[54] J. Scheuer, I. Schwartz, Q. Chen, D. Schulze-Sünninghausen, P. Carl, P. Höfer, A. Retzker, H. Sumiya, J. Isoya, B. Luy, M. B. Plenio, B. Naydenov, and F. Jelezko, Optically induced dynamic nuclear spin polarisation in diamond, NewJ. Phys. **18**, 013040 (2016).

[55] I. Schwartz, J. Scheuer, B. Tratzmiller, S. Müller, Q. Chen, I. Dhand, Z.-Y. Wang, C. Müller, B. Naydenov, F. Jelezko, and M. B. Plenio, Robust optical polarization of nuclear spin baths using Hamiltonian engineering of nitrogen-vacancy center quantum dynamics, Sci. Adv. **4**, eaat8978 (2018).

[56] E. V. Denning, D. A. Gangloff, M. Atatüre, J. Mørk, and C. Le Gall, Collective Quantum Memory Activated by a Driven Central Spin, Phys. Rev. Lett. **123**, 140502 (2019).

[57] D. Pagliero, P. R. Zangara, J. Henshaw, A. Ajoy, R. H. Acosta, J. A. Reimer, A. Pines, and C. A. Meriles, Optically pumped spin polarization as a probe of many-body thermalization, Sci. Adv. **6**, eaaz6986 (2020).

[58] I. Lovchinsky, J. Sanchez-Yamagishi, E. Urbach, S. Choi, S. Fang, T. Andersen, K. Watanabe, T. Taniguchi, A. Bylinskii, E. Kaxiras, P. Kim, H. Park, and M. D. Lukin, Magnetic resonance spectroscopy of an atomically thin material using a single-spin qubit, Science **355**, 503 (2017).

[59] D. Schmid-Lorch, T. Häberle, F. Reinhard, A. Zappe, M. Slota, L. Bogani, A. Finkler, and J. Wrachtrup, Relaxometry and dephasing imaging of superparamagnetic magnetite nanoparticles using a single qubit, Nano Lett. **15**, 4942 (2015).

[60] R. Barends, *et al.*, Superconducting quantum circuits at the surface code threshold for fault tolerance, Nature **508**, 500 (2014).

[61] M. Reagor, *et al.*, Demonstration of universal parametric entangling gates on a multi-qubit lattice, Sci. Adv. **4**, eaao3603 (2018).

[62] A. Soare, H. Ball, D. Hayes, J. Sastrawan, M. Jarratt, J. McLoughlin, X. Zhen, T. Green, and M. Biercuk, Experimental noise filtering by quantum control, Nat. Phys. **10**, 825 (2014).

[63] P. Fernández-Acebal, O. Rosolio, J. Scheuer, C. Müller, S. Müller, S. Schmitt, L. McGuinness, I. Schwarz, Q. Chen, A. Retzker, B. Naydenov, F. Jelezko, and M. B. Plenio, Toward hyperpolarization of oil molecules via single nitrogen vacancy centers in diamond, Nano Lett. **18**, 1882 (2018).